Microstructural evolution of source rocks during hydrocarbon generation: A small-angle-scattering study

A. P. Radlinski and C. J. Boreham
Australian Geological Survey Organization, GPO Box 378, Canberra, Australian Capital Territory 2601, Australia

G. D. Wignall and J.-S. Lin
Center for Small-Angle Scattering Research, Solid State Division, Oak Ridge National Laboratory, Oak Ridge, Tennessee 37831
(Received 13 March 1995; revised manuscript received 30 November 1995)

The evolution of microstructure of shaly source rocks occuring during the natural oil generation is studied by the small-angle neutron and x-ray scattering for length scales 50–2000 Å. The study is performed on a set of rocks with several weight percent organic matter content, forming a natural maturity sequence for hydrocarbon generation. These rocks have been previously analyzed using various geochemical methods. The applicability of small-angle scattering techniques for the quantitative source rock studies is also tested using the laboratory-prepared rocks containing hydrogenated or deuterated eicosane. Although the natural source rocks are five-phase systems, they are perceived by neutrons as quasi-two-phase, which enables straightforward interpretation of the SANS data. The surfaces of immature source rocks are fractal ($D=2.5+/-0.1$) within the entire length scale region, regardless of the organic content. Upon maturation, two distinct fractal regimes develop ($D=2.8+/-0.1$ and $D=2.0+/-0.05$) for the length scales below and above 600 Å, respectively. The SAXS and SANS data are compared with the geochemical thermal maturity indicators and a model of source rock structural evolution is presented. Our data suggest an oil generation scenario according to which hydrocarbons are produced from macerals finely dispersed inside the bulk of the rock and also concentrated on the grain boundaries for grain sizes larger than 600 Å. Upon reaching the thermal conditions necessary for oil generation the small grains crack and release oil into these microfractures, whereas the intergranular macerals produce oil and also wet the interface, thus forming an oil-wet network of conduits for primary migration. [S0163-1829(96)05921-8]

I. INTRODUCTION

Migration of hydrocarbons during the natural petroleum generation process is instrumental for the formation of gas and oil accumulations. The first step in this process, the primary migration within the source rock in which the hydrocarbons are generated, is facilitated by the chemical decomposition of the organic matter in the rock and a consequent microstructural evolution of the inorganic rock matrix. The chemical changes resulting from the thermal maturation of the organic matter in source rocks have been long studied and the processes involved are relatively well understood.[1] By contrast, the microstructural evolution (i.e., microscopic changes in geometry and topology) of the inorganic and organic components of the rocks upon maturation remained unknown, although much speculated about.[2] In this work we present experimental evidence relating microstructural changes to the various stages of maturation for a series of hydrocarbon source rocks.

We study a set of sedimentary rocks forming a natural maturity sequence for hydrocarbon generation. These rocks were found in middle Proterozoic (1400 m.y.) sediments from the Velkerri Formation, McArthur Basin, Northern Territory, Australia.[3] Sampled within the BMR Urapunga 4 well were mudstones and siltstones containing organic-rich intervals of a dispersed marine type-II organic matter.[3,4] These rocks have been subjected to a series of geochemical studies and their chemical evolution is well understood.[4–7] Thermal maturity indicators based on both bulk and molecular-level geochemical techniques indicate that an oil-generation window exists[4,5] at the depth range between 155 and 370 m. Accordingly, we have focused the present study on the rocks originating from this particular interval.

II. EXPERIMENT

A. SAXS and SANS

The microstructure of rocks was probed using the small-angle neutron scattering (SANS) and small-angle x-ray scattering (SAXS) techniques. These techniques are well suited for analyzing the structural features ranging in size from 10 to 2000 Å. No other nondestructive method of analysis can provide structural information about rocks over this scale range.

The SANS data were collected on the W. C. Koehler 30 m SANS facility[8] at the Oak Ridge National Laboratory (ORNL) with a 64×64 cm^2 area detector and cell (element) size about 1 cm^2. The neutron wavelength was 4.75 Å ($\Delta\lambda/\lambda\cong5\%$) and a range of sample-detector distances (1.3 to 19.1 m) were used to give a Q-range of $0.003<Q<0.5$ Å^{-1}. The data were corrected for instrumental backgrounds and detector efficiency on a cell-by-cell basis, prior to radial (azimuthal) averaging. The net intensities were converted to an absolute ($\pm4\%$) differential cross section $[I(Q)=d\sigma/d\Omega(Q)]$ per unit sample volume (in units of cm^{-1}) by comparison with precalibrated secondary standards, based on the

measurements of the beam flux, vanadium incoherent cross section, the scattering from water and other reference materials.[9] The efficiency calibration was based on the scattering from light water and this led to angle-independent scattering for vanadium, H-polymer blanks and water samples of different thicknesses in the range 1–10 mm.

The transmission of the sample was measured in a separate experiment[10] by collimating the beam with slits (irises) 1 cm in diameter, separated by a distance about 7.5 m. A strongly scattering sample, porous carbon, was placed at the sample position to spread the beam over the whole detector, placed at the sample-detector distance about 10 m. Without the carbon in position, the beam would either be blocked by the beam stop or concentrated in a few detector cells, with the possibility of saturating or damaging the detector. The total count summed over the whole detector ($>10^5$) was recorded in a time period of 1 min and the sample being measured was placed over the source slit, thus attenuating the beam. The count was repeated over the same time interval and the transmission is given by the ratio of the two counts after minor corrections ($<0.1\%$) for the blocked-beam background due to electronic noise, cosmic rays, etc. In this geometry only scattering from the sample at Q values less than 10^{-3} Å^{-1} can enter the second iris and be scattered by the porous carbon and hence be counted by the detector.

The SAXS experiments were performed on the ORNL 10 m SAXS instrument,[11] with sample-detector distances of 1.1–5.1 m using $Cu_{K\alpha}$ radiation ($\lambda=1.54$ Å) and a 20×20 cm^2 area detector with cell (element) size of 3 mm. Corrections were made for instrumental backgrounds and detector efficiency (via an Fe^{55} standard which emits γ rays isotropically) on a cell-by-cell basis. The data were radially (azimuthally) averaged in the Q range $0.004<Q<0.5$ Å^{-1}, and converted to an absolute differential cross section by means of precalibrated secondary standards.[12]

B. Samples

The source rock samples were obtained from seven depth intervals within the Velkerri Formation, covering a reasonable range of maturity (Table I). From each interval two samples were cut out, one oriented parallel and the other perpendicular to the bedding plane. A typical thickness of the SANS samples was 6–8 mm. Samples for SAXS experiments were prepared from thin slices of rock cut off the corresponding SANS samples and their thickness was of the order of 0.1 mm. As expected, both SAXS and SANS spectra were anisotropic for samples cut out perpendicular to the bedding plane, indicating a different pore size in the vertical and horizontal direction. The pores were vertically compressed and the anisotropy ratio was 2:1. Only data taken from rocks cut out parallel to the bedding plane are analyzed in this work. These spectra were fully isotropic.

Three types of artificial rocks were made using a lean shale of known chemical composition as the starting material (samples 82S, 83S, and 84S, Table I). The shale was crushed to fine powder and annealed in air for 24 h at 600 °C in order to remove the natural organic components. Eicosane (99% Aldrich Chemical Co.) and deuterated eicosane (98.8 at. % D, MSD isotopes) were dissolved in dichloromethane and thoroughly mixed with the annealed shale powder to the required concentration. Excess solvent was removed using a vacuum evaporator. The pure shale powder and the powders mixed with eicosane and deuterated eicosane were then pressed into pellets of appropriate thickness for SAXS and SANS studies.

TABLE I. Rocks used in the SANS and SAXS study. The first even rocks originate from the natural maturity sequence probed by the BMR Urapunga 4 well. Samples 82S, 83S, and 84S were artificial laboratory preparations.

Sample number	Depth interval (m)	Equivalent vitrinite reflectance (%)	Total organic carbon (%)
13S	132.60	0.73	6.61
15S	155.65	0.75	5.28
17S	155.70	0.75	0.67
19S	157.30	0.77	8.68
21S	216.90	0.81	3.88
23S	324.60	1.13	5.81
27S	346.55	1.19	2.91
82S	Artificial	n/a	None
83S	Artificial	n/a	5.0 Eicosane
84S	Artificial	n/a	3.7 Deuterated Eicosane

III. THEORETICAL BACKGROUND

The contribution of different phases to the total SANS scattering cross section can be determined from the values of the corresponding scattering length densities, $\rho_n(\mathbf{r})$. The scattering amplitude for neutrons, $A(\mathbf{Q})$, is related to $\rho_n(\mathbf{r})$ by

$$dA(\mathbf{Q})=\rho_n(\mathbf{r})\exp(-i\mathbf{Qr})dV, \tag{1}$$

where $\mathbf{Q}$ is the scattering vector and dV the scattering volume element. The scattering length density depends on the coherent scattering lengths of individual nuclei in the following way:

$$\rho_n(\mathbf{r})=(1/V)\Sigma_i b_i\delta(\mathbf{r}-\mathbf{r}_i), \tag{2}$$

where the summation is extended over all the nuclei, i, contained in the volume V. For x rays, the scattering amplitude is

$$dA(\mathbf{Q})=I_e\rho_e(\mathbf{r})\exp(-i\mathbf{Qr})dV, \tag{3}$$

where $I_e=(e^2/mc^2)$ is the scattering amplitude for a single electron and $\rho_e(\mathbf{r})$ is electronic density (i.e., number of electrons per unit volume). By comparison of relations (1) and (3) one can see that the product $I_e\rho_e(\mathbf{r})$ plays the same role in SAXS as the scattering length density $\rho_n(\mathbf{r})$ does in SANS.

Real rocks may contain several macroscopic phases that can be distinguished in the small-angle scattering experiments. A single phase may be a fine mixture of a number of chemical compounds, labeled with a running index j, each compound containing a number of different atoms (isotopes), labeled with a running index i. The scattering length density

for such a single-phase, complex mixture of molar mass M can be calculated if its density and chemical composition are known:

$$\rho_n=(N_A d/M)[\Sigma_j p_j(\Sigma_i s_i b_i)_j], \tag{4}$$

where N_A is the Avogadro's number, d is density, s_i is the proportion by number of nucleus i in the compound j, and p_j is the proportion by molecular number of the compound j in the mixture. The product $I_e\rho_e$ can by simply calculated as

$$I_e\rho_e=(N_A d/M)N_e I_e, \tag{5}$$

where N_e is the number of electrons per one ''supramolecule'' of composition as in the square brackets in Eq. (4).

The quantity measured in a small-angle scattering experiment is the scattered intensity $I(Q)$, equivalent to the differential cross section $d\sigma/d\Omega$:

$$I(Q)=A(Q)A^*(Q)=C_0\int_v \gamma(\mathbf{r})\exp(-i\mathbf{Qr})dV, \tag{6}$$

where $\gamma(\mathbf{r})$ is the density-density correlation function; C_0 is unity for neutrons and I_e^2 for x rays. For a multiphase system the correlation function has the form[13,14]

$$\gamma(\mathbf{r})=\sum_{i,j} P_{ij}(\mathbf{r})(\rho_i-\rho_0)(\rho_j-\rho_0), \tag{7}$$

where $\rho_i=\rho_{ei}$ or ρ_{ni}, ρ_0 is the volume average of ρ_e or ρ_n, indices i and j indicate separate phases of the system and $P_{ij}(\mathbf{r})$ is the probability that a point at distance $\mathbf{r}$ away from a randomly selected point in phase i happens to be in phase j.

The major difficulty in the interpretation of small-angle scattering data obtained from rocks with organic content is the multiphase character of the scattering medium. Natural source rocks are five-phase systems, composed of (i) inorganic rock fabric, (ii) organic macerals, (iii) oil, (iv) water, and (v) gas and/or voids. Scattering length densities for neutrons and the $I_e\rho_e$ products for x rays calculated for these five phases using Eqs. (4) and (5) are shown in Fig. 1. It follows that the BMR Urapunga 4 source rocks are approximately two-phase for SANS, with a little contrast between the shale and maceral phase as well as between voids, oil, and water. This is an important coincidence, since the interpretation of small-angle scattering data is much more straightforward for two-phase systems than for multiphase ones. It is also clear from Fig. 1 that x rays perceive the BMR Urapunga 4 rocks as four-phase. There is very little difference between oil and water scattering cross section for both neutrons and x rays.

It is a general theoretical result that small-angle scattering from ideal fractals results in a power-law dependence of the scattered intensity (differential cross section) I on the scattering vector Q. For real (i.e., material) two-phase fractal objects the power-law scattering on theoretical grounds is expected within the Q region for which $Ql_{\max}\gg 1$ and $Ql_{\min}\ll 1$.[15–17] These two inequalities ascertain that the range of Q is such that the scale of length probed by x rays or neutrons is smaller than the object's total linear diameter $l_{\max}$ but larger than the size $l_{\min}$ of the individual building block.

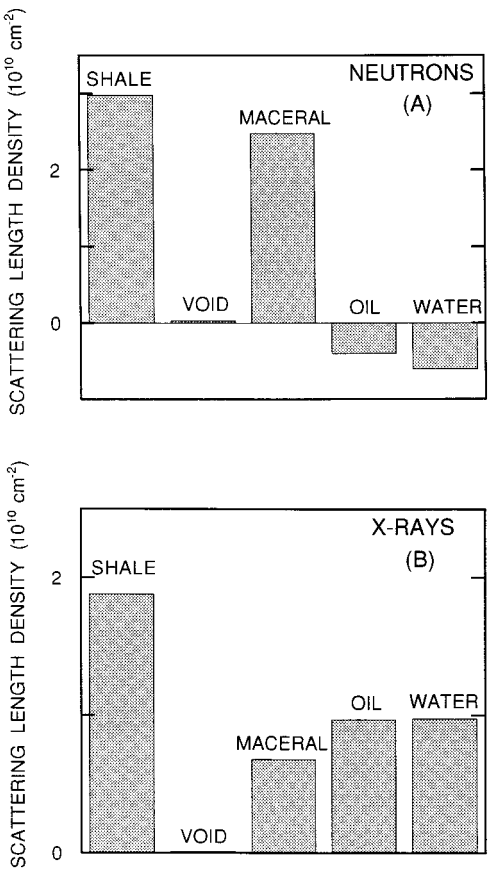

FIG. 1. (a) Neutron (ρ_n) and (b) electron ($I_e\rho_e$) scattering length densities for the five phases present in BMR Urapunga 4 source rocks calculated from the known chemical composition.

Since there may be various limitations for the range of scale over which a given physical object is self-similar, it is usually assumed that in order to justify the notion of a fractal the appropriate geometrical properties should extend over at least 1 order of magnitude of the length scale. As the experimental Q range is also limited (in this work it extends over 2 orders of magnitude), the upper- and lower-limit cutoffs may affect the experimental data and distort the apparent fractal dimensions of the system. Such a situation for polydisperse fractal aggregates of Hausdorff dimensionality close to 2 has been recently discussed in detail by Nicolai *et al.*[18] Therefore, below we give a brief overview of theoretical approach to the size limit effects which may be relevant to rocks.

The upper size limit to a fractal structure can be introduced in a natural way at the level of the correlation function. For mass fractals it has been done by Sinha *et al.*[19] who proposed the correlation function of a form

$$\gamma(r)\propto\exp(-r/\eta)r^{D_m-3}, \tag{8}$$

where η (equivalent to $l_{\max}$ in our previous notation) is the correlation length. The first (exponential) term reflects the upper-size-limit-related decay of fractal properties, the second (power) term is the correlation function for a perfect fractal,[20] and D_m is the fractal (Hausdorff) dimension of the object. The Fourier transform [Eq. (6)] of $\gamma(\mathbf{r})$ gives

$$I(Q)=Q^{-1}\Gamma(D_m-1)\,\eta^{D_m-1}[1+(Q\eta)^2]^{(1-D_m)/2}\times\sin[(D_m-1)\arctan(Q\eta)]. \quad (9)$$

Such a form of scattering has been reported for silica particle aggregates.[20] For $\eta Q\gg 1$ the limiting behavior is

$$S(Q)=Q^{-D_m}\Gamma(D_m-1)\sin[(D_m-1)(\pi/2)], \quad D\leqslant 3 \quad (10)$$

which is an $I(Q)=\text{const}\ Q^{-D_m}$ power law expected for perfect mass fractals. For D_m close to 3, which is observed for some of the rocks studied by us, the convergence between (9) and (10) occurs for $\eta Q>2$. This means that the transitional Q range near the upper size limit is relatively narrow. This is not the case, however, for polydisperse aggregates of D_m close to 2 discussed in Ref. 17.

The correlation function for real surface fractals with the upper limit ξ for the range of scale invariance (equivalent to $l_{\max}$) was proposed by Mildner and Hall,[21] based on the correlation function of Bale and Schmidt[22] for perfect surface fractals:

$$\gamma(r)=\exp(-r/\xi)[1-C(r/\xi)^{3-D_s}], \quad (11)$$

where $C=S_0/4\phi(1-\phi)V$, V is the sample volume, ϕ is porosity, and S_0 a constant of area dimension.[22] For a smooth interface S_0 is the interfacial surface area. A Fourier transform of (11) leads to

$$S(Q)=Q^{-1}\Gamma(5-D_s)\xi^{5-D_s}[1+(Q\xi)^2]^{(D_s-5)/2}\times\sin[(D_s-1)\arctan(Q\xi)]. \quad (12)$$

For $\xi Q\gg 1$, the limiting behavior is

$$S(Q)=Q^{D_s-6}\Gamma(5-D_s)\sin[(D_s-1)(\pi/2)], \quad 2\leqslant D<3 \quad (13)$$

which is an $I(Q)=\text{const}\ Q^{6-D_s}$ power law and reduces to the Porod limit for $D_s=2$. In Fig. 2 we illustrate that for practical purposes the transition from (12) to (13) is complete for $\xi Q>2$.

The form of (11) is the consequence of assumption that the fractal surface is self-affine and that its roughness scales in such a way that the surface area per unit volume at roughness scale r, $S(r)$, has the form[23]

$$S(r)=S_0(r/\xi)^{2-D_s}. \quad (14)$$

This enables one to calculate the surface area per unit volume at any scale length once the ''smooth'' specific surface S_0 (i.e., that measured at the length scale ξ) is known.

The question of lower size limit effect is related to the size ($l_{\min}$) and shape of the building blocks (or elementary units) of a real fractal object. These can be atoms, molecules, molecular clusters, or larger objects. In the case of rocks studied here the building blocks are clusters of a large number of finely dispersed particles of mineral and organic matter. The individual components of these rocks can be easily resolved in the x-ray-diffraction spectra, but in the small-angle region only the structure factor of elementary unit may be possibly seen (in the large-Q limit for $Ql_{\min}>0.3$).[18] In some cases there may not be a clearcut transition from fractal scattering to the individual particle scattering, depending on the particular shape of the building blocks. As the rocks studied here are strong fractal scatterers, the lower size limit effects are relatively weak (although detectable). Independent microstructural information on rocks is very limited and in order to avoid arbitrary assumptions we perform the fractal analysis of our data in such a Q range where the lower size limit effects are negligibly small compared to the fractal scattering intensity.

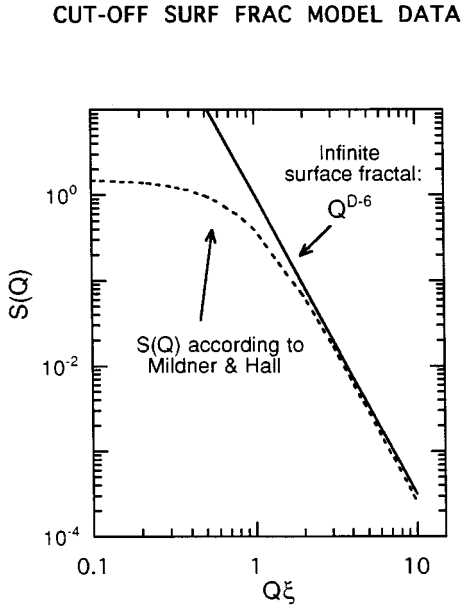

FIG. 2. Form factor for a real surface fractal with correlation length ξ. Transition to the power-law behavior takes place for $\xi Q>2$.

There may be both surface and mass fractal structures present in a rock. Surface fractals are bulk objects with rough surface, the roughness being scale invariant within the certain range of sizes. For surface fractals the majority of building blocks remain in the bulk. The *surface area* is proportional to R^{D_s}, where the surface fractal dimension D_s remains within the limits $2\leqslant D_s<3$ and R is the length of the measuring stick (linear scale). A good example of surface fractal could be planet Earth with its rough surface morphology (D_s may vary from 2 to 2.5, depending on the position and length scale). For mass fractals the majority of building blocks are exposed to the surface. The volume and, consequently, the *mass* of a mass fractal is proportional to R^{D_m}, where the mass fractal dimension D_m can be no larger than 3. An example could be a river system or a network of cracks in a solid. In the latter case the relative position of matter and voids is reversed and a name of pore fractal is sometimes used.

As discussed above, the specific form for the small-angle scattering law has been derived for the surface fractals[22,24,25] and mass fractals,[15,17,26] both ideal and real. For both mass and surface fractals the result $I\propto Q^{-S}$ has been obtained, where the magnitude of the exponent S is D_m and $6-D_s$ for the mass and surface fractals, respectively. This result is valid for real fractals only in the limited Q range, reflecting the existence of the upper and lower size limits for the fractal behavior. Since $2\leqslant D_s<3$ and $D_m\leqslant 3$, $S<3$ for mass fractals and $3<S\leqslant 4$ for surface fractals. Therefore, the slope of the small-angle scattering curve on the log-log scale directly in-

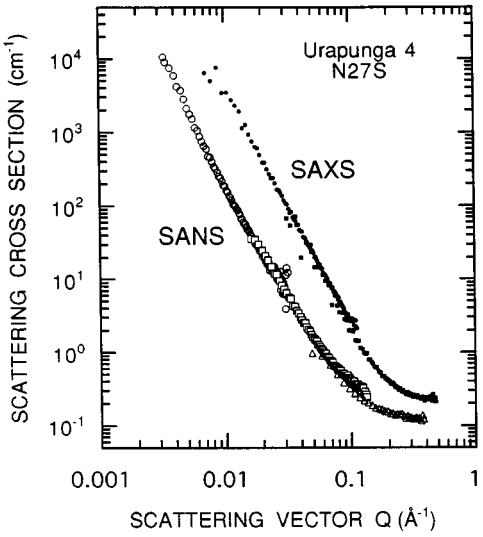

FIG. 3. log $I(Q)$ vs log Q for SANS and SAXS data for sample 27S. The different symbols refer to different sample-detector distances.

dicates whether the scattering occurs from a surface or mass fractal, provided the system is two-phase. For multiphase systems the relationship between the differential cross section and the density-density correlation functions is more complex [Eqs. (6) and (7)] and the above result is generally not valid. Note that for a smooth, nonfractal surface $D_s=2$ and the classical Porod limit, $I(Q)\propto Q^{-4}$, is reproduced.

IV. RESULTS AND DISCUSSION

Typical SANS and SAXS spectra covering the Q range 3.2×10^{-4}–0.5 Å^{-1} exhibit a monotonuously decreasing scattering intensity with increasing Q value (Fig. 3). For larger Q values ($Q>0.032$ Å^{-1}) gradual flattening out of scattering curves is observed. This is caused by the presence of low-level scattering background which may originate from two separate phenomena.

First, for SANS there certainly is a significant contribution from the incoherent scattering on hydrogen nuclei, since the flattening effect is markedly less distinct for samples containing deuterated hydrocarbons. The incoherent background may be estimated by empirical methods[10] and when a correction for this component was made by subtracting a flat background of about 0.01–0.15 cm^{-1}, the SAXS and SANS curves were found to have similar shapes even for the larger Q values. This was confirmed by SANS experiments made on artificial rocks containing hydrogenated or deuterated eicosane (samples 83*S* and 84*S*, Table I and Fig. 4). Second, there is an additional background neutron scattering different from the incoherent component, which varies from sample to sample in the range 0.04–0.5 cm^{-1} in a way apparently unrelated to the geochemical characteristics.

This latter contribution, which also causes the flattening out of the SAXS curves in the large-Q region observed both for the hydrogenated as well as deuterated samples, is likely to originate from the small-scale nuclear and electronic density inhomogeneities that have developed during the rock deposition, diagenesis, and/or maturation. This is basically

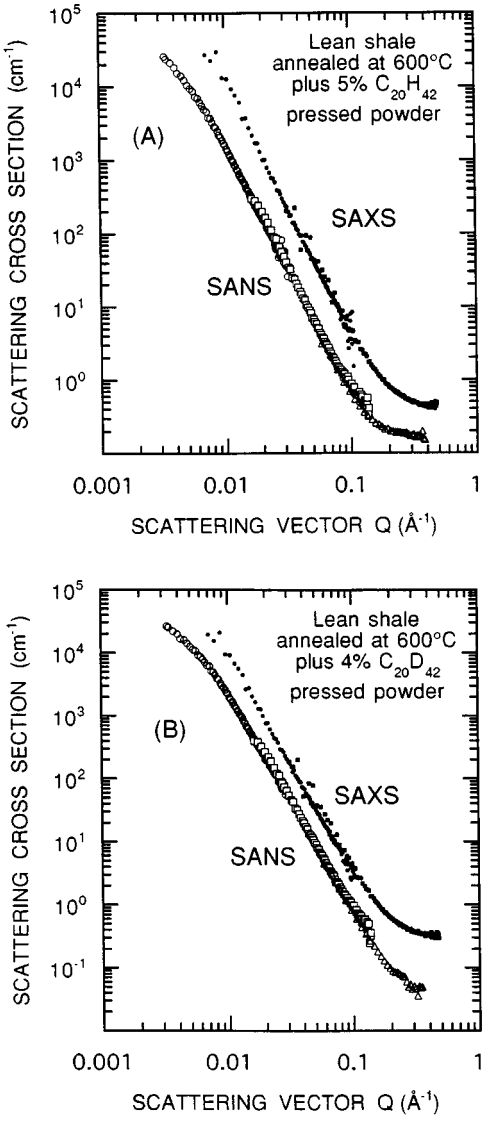

FIG. 4. Comparison of SANS and SAXS data for artificial rocks mixed with (a) eicosane and (b) deuterated eicosane. The SAXS data are similar in both cases but there is a difference between the SANS data at the highest-Q values.

the lower size limit effect. From the Q value of its onset one can estimate the building block size to be about 30–100 Å, but there is no structural information to support any specific building block shape model. In order to avoid speculative interpretation, the analysis presented in this report is limited to the region $Q<0.032$ Å^{-1}. In this range the large-Q background is at least 2 orders of magnitude smaller than the fractal scattering and can be neglected.

Examples of SANS and SAXS log-log plots for the immature (17S) and mature (27S) rock are shown in Fig. 5. In the range $3.2\times10^{-4}<Q<3.2\times10^{-2}$ Å^{-1} these spectra can be described by a power law for the low maturity rocks and two various power relationships for more mature samples. Behavior similar to that shown in Fig. 5 is observed for all the BMR Urapunga 4 source rocks studied by us. The values of the slope (giving the power-law exponent) were determined from the SANS and SAXS log-log plots using a least-squares-fitting procedure.

The plot of slope versus maturity for the whole BMR

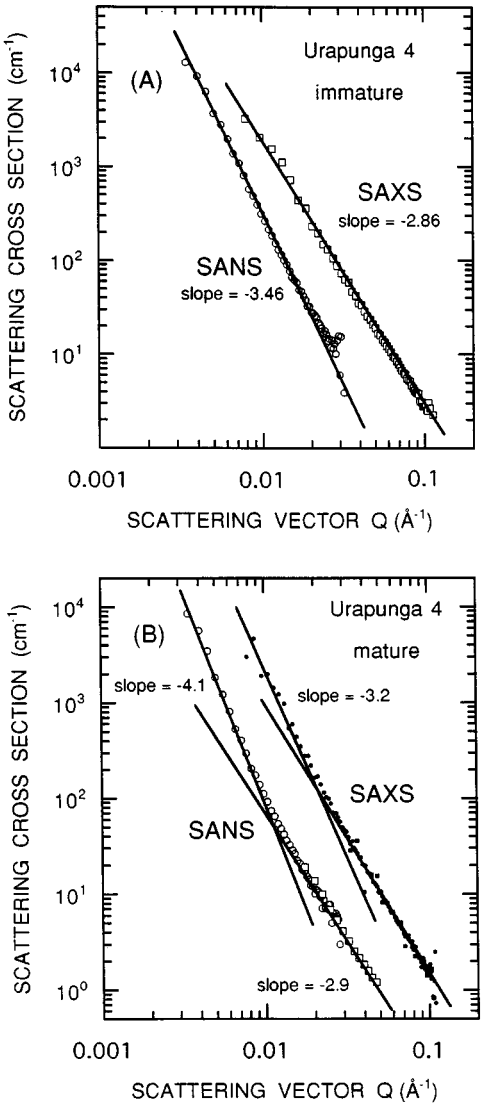

FIG. 5. (a) SAXS and SANS data ($3\times10^{-3}<Q<3\times10^{-2}$ Å^{-1}) for the immature source rock 17S; (b) SAXS and SANS data ($3\times10^{-3}<Q<3\times10^{-2}$ Å^{-1}) for a mature source rock 27S.

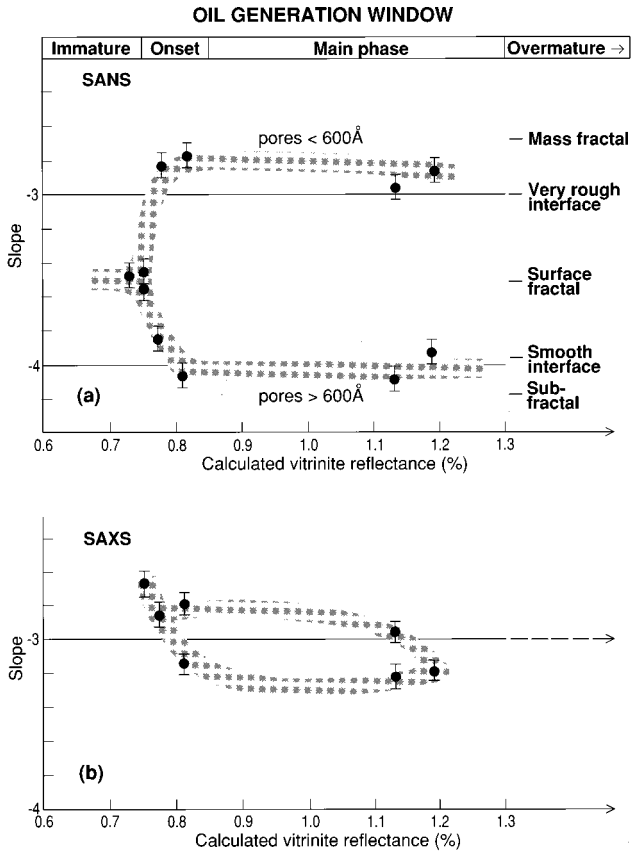

FIG. 6. Plot of the slope of small-angle scattering curve vs maturity in the Q range as in Fig. 5: (a) SANS data, (b) SAXS data. See text for description.

Urapunga 4 series is shown in Fig. 6(a) for SANS and Fig. 6(b) for SAXS data. The thermal maturity of each sample has been quantified by calculating its equivalent vitrinite reflectance by correlating it with the methyl phenanthrene index (MPI) previously determined for the BMR Urapunga 4 rocks and correlated to the widely used vitrinite reflectance (VR) by the relation $VR=0.7MPI+0.22$.[4] The oil-generation window subdivision as used in petroleum geology is displayed above the plot and should be referred to the corresponding values of the vitrinite reflectance shown on the abscissa. The ordinate is the slope of the SANS [Fig. 6(a)] or SAXS [Fig. 6(b)] curve. If the curve has two different slopes in the Q range used, both values are plotted for the corresponding value of vitrinite reflectance. The change of slope for the SANS curves occurs for the more mature samples systematically near the value of $Q=0.01$ Å^{-1}, which corresponds to the real space distance $2\pi/Q$ of about 600 Å.

The direct observations with the atomic force microscopy of the cleaved BMR Urapunga 4 rock surfaces demonstrate a rough character of the rock fabric on scales varying from 100 Å to 1 μm.[27] This strongly indicates that the scattering interface may be of fractal character, similarly to the situation previously reported for several different types of rock. Some examples of previous small-angle scattering studies on sedimentary rocks are Wong *et al.*[28] on Coconino sandstone, Portland sandstone, and Frio shale; North *et al.*[29] on Bakken shale; Bale and Schmidt[22] on lignites and other coals; and Schmidt[17] on river Lahn sediments.

The plot of slopes obtained from SANS data [Fig. 6(a)] pertains to a quasi-two-phase system and, therefore, can be directly interpreted in terms of fractal geometry in the two-phase approximation. This can be done at the cost of losing distinction between the solid rock components as well as between the empty pores and the gas-oil-water phase. The inorganic rock matrix and the organic maceral are thus incorporated into a single solid supraphase whereas the empty pores, water, and hydrocarbons form a fluid supraphase.

For the low maturity samples (13S,15S,17S) a single slope of -3.5 $+/-0.1$ is observed. The SANS spectrum for sample 17S does not significantly differ from the other two spectra, although this rock has a very small organic carbon content of 0.67 wt % compared to 3–8.7 % for other samples in the BMR Urapunga 4 series (Table I). A slope of -3.5 indicates a surface-fractal geometry of the solid-fluid interface, which does not seem to be influenced by the presence or absence of the organic matter at this low maturity stage of the rock evolution.

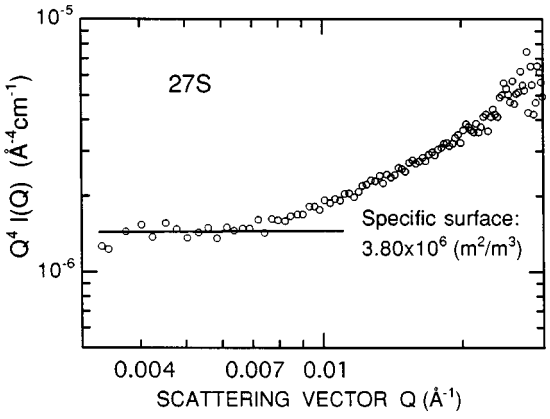

FIG. 7. Porod plot for the mature sample 27S. The ''smooth'' specific surface derived from the plot is 1.55 m^2/g.

With increased maturity of the source rocks, just at the point where the vitrinite reflectance indicates an onset of the oil-generation window, there is a very significant branching of the slope values in Fig. 6(a). This reflects the fact that the SANS slopes for the length scales 50–600 Å and 600–2000 Å are different. For the smaller scale, the slope increases to $-2.8 +/-0.1$ from the original value of -3.5 for the immature source rock, thus crossing over the border value of -3 into the region of pore fractals. This pore fractal may be interpreted as a system of interconnected microcracks created as a result of petroleum generation.[2] On the scale 600–2000 Å the slope approaches -4, which is the classical Porod limit for a smooth interface. Interestingly, the 600 Å size boundary broadly corresponds to the distinction between meso- and macropores, which have been shown to have differing levels of petroleum saturation within the oil window.[30]

For immature source rocks we observe no flattening out of the scattering intensity in the small-Q region. There is also no transition to Porod limit anywhere in the experimental Q range, which indicates that the fractal roughness of the solid-fluid interface persists down to the building block scale range. Therefore, neither ξ nor S_0 can be directly determined and one can only estimate that $\xi > 2000$ Å. For the mature rocks, however, the roughness is removed in the small-Q region and one can determine the specific surface S_0 (see Porod plot in Fig. 7):

$$S_0 = \lim_{Q\to\infty}\{Q^4 I(Q)/[2\pi(\rho_1-\rho_2)^2]\}. \qquad (15)$$

The interface appears smooth in the linear size range 900–2100 Å, where the linear dimension x is related to the corresponding Q value according to $x = 2\pi/Q$. Using the contrast of $(\rho_1-\rho_2)^2 = 8.41\times10^{20}$ cm^{-4} (close to the shale-void value, Fig. 1) and the measured rock density of 2.45 g/cm^3, one obtains the ''smooth'' specific surface: $S_0 = 3.8\times10^6$ m^2/m^3 or 1.55 m^2/g. This is a rather small value. Although there are no data for Urapunga 4 rocks, the typical specific areas for shales[1] are known to vary between 10 and 60 m^2/g between depths 500–3500 m. However, these results have been obtained using mercury porosimetry and gas-adsorption techniques, in which the probe size is atomic. Consequently, they correspond not to S_0, but $S(r)$ of Eq. (14) for r equal several Å. Substituting to Eq. (14) $r = 5$ Å, $\xi = 2\pi/Q_{\max} = 900$ Å, and $D_s = 3$ (maximum fractal dimension for surface fractals), one estimates $S(r) = 44$ m^2/g for the mature Urapunga 4 rocks, in good agreement with the other shale data. The quantity $Q_{\max}$ used to estimate the lower limit of ξ is the upper Q limit of the Porod region (and the lower Q limit for the interface roughness) determined from Fig. 7.

One can perform similar calculations for the immature Urapunga 4 rocks assuming that the ''smooth'' specific surface S_0 is the same as for mature rocks. Given the geological context and interpretation of our data (discussed below) this seems to be a justified assumption. For immature samples, $D = 2.5$ and the lower limit of ξ is determined by the upper limit of experimental Q range: $\xi > 2000$ Å. Using $D = 2.5$, $\xi = 2000$ Å and $r = 5$ Å one obtains $S(r) = 31$ m^2/g, which is again within the range expected for shales. The specific surfaces for both mature and immature rocks are only estimates, however, owing to the approximate values of ξ used in our calculations.

The SANS and SAXS data obtained from samples cut out perpendicular to the bedding plane indicate that Urapunga 4 source rocks are anisotropic. For these rocks, the isointensity scattering profiles are roughly elliptical (with the long-to-short axis ratio about 2:1) which is characteristic of microstructural inhomogeneities having azimuthal symmetry about the vertical axis.[21] This indicates that the pore space is flattened in the vertical direction, which is expected on the geological grounds. Such deformation of the pore space may affect the values of specific surface estimated above for the ''in-bedding-plane'' component of the rock microstructure, but is unlikely to change them very significantly. More significantly, it does not influence the overall picture of the microstructural evolution of source rocks in response to thermal maturation, as discussed below.

Our interpretation of Fig. 6(a) in the geochemical context of source rock thermal maturation is as follows. The organic matter is originally finely dispersed in the inorganic matrix of immature source rock. Because of little contrast for neutrons between the inorganic and organic solid components of the rock, the scattering occurs predominantly on the solid-fluid interface. The interface with the pore space is of the surface fractal character, which is equivalent to a polydisperse system of pores.[31,32]

Upon burial, compaction and heating the maceral (kerogen) undergoes a series of complex chemical reactions leading to a breakup of large organic molecules and formation of hydrocarbons.[1] The simultaneous increase of the pressure results in a buildup of internal stress that eventually causes major restructuring of the pore space. It follows from Fig. 6(a) that the restructuring occurs very rapidly upon maturation at the onset of the oil-generation window in a twofold way: by creating a system of microcracks inside the solid phase regions smaller than about 600 Å and by smoothing out the solid-fluid interface on scales larger than 600 Å. The microcracks provide conduits for the release of intragranular pressure and also accommodate the transport of fluid hydrocarbons out of the grains.[29,33]

The smoothing out of the solid-fluid interface cannot be a purely mechanical effect and probably involves either (i) a wetting of the inorganic rock matrix by the maceral which begins to melt due to the elevated temperature and stress at the onset of oil generation or (ii) a redistribution of newly

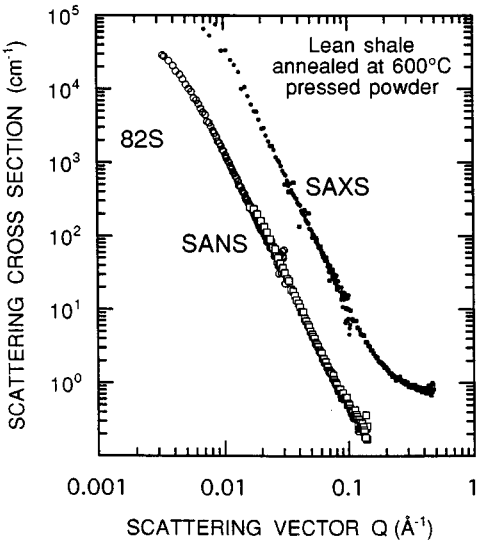

FIG. 8. Comparison of SANS and SAXS data for the two-phase artificial rock 82S.

formed macerals at the larger size grain boundaries, or both. Process (i) would indicate that the solid organic matter may be deposited in the immature source rocks at two different locations: as a finely dispersed phase throughout the whole rock volume and at high concentration on the grain boundaries for grains larger than some 600 Å across. Alternatively, process (ii) would be the consequence, on the submicroscopic scale, of the process of petroleum generation which is known to be accompanied by about 50% mass loss of maceral and related change in maceral configuration on the optically accessible size scale (about 10 000 Å).[4,7,34] In any case, the organic matter distribution and the inorganic matrix structure must reflect of details of depositional and diagenetic process for the accumulation of inorganic and organic matter in the low energy, reducing marine environment of the McArthur Basin some 1.4 billion years ago.

The importance of the validity of the two-phase approximation for the interpretation of small-angle scattering data is well illustrated by comparing Figs. 6(a) and 6(b). The two figures are clearly different, whereas *in the two-phase approximation* the SAXS and SANS scattering intensities are theoretically expected to be proportional to each other and, consequently, the scattering curves should be parallel. We have verified this prediction using the artificial rock 82S with no organic component (Fig. 8). In such a rock only two phases (inorganic matrix and voids) are present and the intensity ratio of the x-ray to neutron scattering equal to 31.7 was calculated from the known chemical composition. The agreement with the experimentally determined ratio of 30 is very good.

The SAXS data used to create Fig. 6(b) were taken using slices of rock cut off the corresponding SANS samples. Because of the largely differing values of the electronic density for different phases ($I_e\rho_e$ in Fig. 1) these data pertain to a truly four-phase system. The SANS and SAXS intensities are not proportional to each other any more and the slope versus maturity plot [Fig. 6(b)] cannot be directly interpreted in this case, although it retains some of the features of Fig. 6(a). In general, for quantitative analysis of a four-phase system a detailed knowledge of the composition and spatial distribution of each phase is required.

V. CONCLUSIONS

Shaly hydrocarbon source rocks are multiphase, natural random systems containing both the organic and inorganic components. In this work, SAXS and SANS techniques have been tested using the two- and three-phase artificial rock samples prepared in laboratory and then applied to a study of source rocks forming a natural maturity sequence for hydrocarbon generation. Because of the specific values of the scattering length densities the neutron scattering data could be interpreted in the two-phase approximation, thus for the first time providing a *direct* insight into the microstructural evolution of source rocks during the oil-generation process and, consequently, the mechanism of primary migration.

The SANS results for BMR Urapunga 4 source rocks indicate that these are dynamic fractal systems, undergoing subtle microstructural changes caused primarily by the chemical breakdown of the organic component. Our data suggest an oil-generation scenario according to which hydrocarbons are produced from macerals finely dispersed inside the bulk of the rock and also concentrated on the grain boundaries for grain sizes larger than 600 Å. Upon reaching the thermal conditions necessary for oil generation the small grains crack and release oil. The intergranular maceral softens and its interface with the fluid phase (voids, oil and water) becomes smooth. Simultaneously, an oil-wet network of conduits for primary migration forms inside the rock.

ACKNOWLEDGMENTS

The research at Oak Ridge was supported by the Division of Materials Sciences, U.S. Department of Energy under Contract No. DE-AC05-84OR21400 with Martin Marietta Energy Systems Inc. One of us (A.P.R.) appreciates discussions with L. Barré and D. Espinat.

[1] B. P. Tissot and D. H. Welte, *Petroleum Formation and Occurrence* (Springer-Verlag, Berlin, 1984).

[2] U. Mann, in *Geofluids: Origin, Migration and Evolution of Fluids in Sedimentary Basins*, edited by J. Parnell, Geological Society Special Publication No. 78 (Geological Society, London, 1994), pp. 233–260.

[3] M. J. Jackson and R. Raiswell, Precambrian Res. **54**, 81 (1991).

[4] I. H. Crick, C. J. Boreham, A. C. Cook, and T. G. Powell, AAPG Bull. **72**, 1495 (1988).

[5] C. J. Boreham, I. H. Crick, and T. G. Powell, Org. Geochem. **12**, 289 (1988).

[6] R. E. Summons, T. G. Powell, and C. J. Boreham, Geochim. Cosmochim. Acta **52**, 1747 (1988).

[7] I. H. Crick, Aust. J. Earth Sci. **39**, 501 (1992).

[8] W. C. Koehler, Physica (Utrecht) **137B**, 320 (1986).
[9] G. D. Wignall and F. S. Bates, J. Appl. Cryst. **20**, 28 (1986).
[10] W. S. Dubner, J. M. Schultz, and G. D. Wignall, J. Appl. Cryst. **23**, 469 (1990).
[11] G. D. Wignall, J. S. Lin, and S. Spooner, J. Appl. Cryst. **23**, 241 (1990).
[12] T. P. Russell, J. S. Lin, S. Spooner, and G. D. Wignall, J. Appl. Cryst. **21**, 629 (1988).
[13] P. Debye, H. R. Anderson, and H. Brumberger, J. Appl. Phys. **28**, 679 (1957).
[14] J. Goodisman and H. Brumberger, J. Appl. Cryst. **4**, 347 (1971).
[15] J. E. Martin and A. J. Hurd, J. Appl. Cryst. **20**, 61 (1987).
[16] J. Teixeira, J. Appl. Cryst. **21**, 781 (1988).
[17] P. W. Schmidt, in *The Fractal Approach to Heterogeneous Chemistry*, edited by D. Avnir (Wiley and Sons, New York, 1989), p. 67.
[18] T. Nicolai, D. Durand, and J-C. Gimel, Phys. Rev. B **50**, 16 357 (1994).
[19] S. K. Sinha, T. Freltoft, and J. Kjems, in *Kinetics of Aggregation and Gelation*, Proceedings of the International Conference, Athens, GA, edited by F. Family and D. P. Landau (Elsevier, New York, 1984), p. 71.
[20] D. W. Schaefer and K. D. Keefer, Phys. Rev. Lett. **53**, 1383 (1984).
[21] D. F. R. Mildner and P. L. Hall, J. Phys. D **19**, 1535 (1986).
[22] H. D. Bale and P. W. Schmidt, Phys. Rev. Lett. **53**, 596 (1984).
[23] A. J. Allen, J. Appl. Cryst. **24**, 624 (1991).
[24] J. K. Kjems and P. Schofield, *Scaling Phenomena in Disordered Systems*, Vol. 133 of NATO Advanced Study Institute, Series B: Physics (Plenum, New York, 1985), p. 141.
[25] J. E. Martin, J. Appl. Cryst. **19**, 25 (1986).
[26] T. A. Witten and L. M. Sander, Phys. Rev. Lett. **47**, 1400 (1981).
[27] A. P. Radlinski, E. Z. Radlinska, and G. Rouquet (unpublished).
[28] P.-Z. Wong, J. Howard, and J.-S. Lin, Phys. Rev. Lett. **57**, 637 (1986).
[29] A. N. North, J. C. Dore, R. H. Keenan, A. R. Mackie, A. M. Howe, B. H. Robinson, and C. Nave, Nucl. Instrum. Methods Phys. Res. B **34**, 188 (1988).
[30] U. Mann, in *The European Oil and Gas Conference: A Multidisciplinary Approach in Exploration and Production R & D*, edited by G. Imarisio, M. Frias, and J. M. Bemtgen (Graham and Trotman, London, 1990), pp. 142–154.
[31] P. Pfeifer and D. Avnir, J. Chem. Phys. **79**, 3558 (1983).
[32] P. W. Schmidt, J. Appl. Cryst. **15**, 567 (1982).
[33] L. C. Price, J. Petr. Geol. **12**, 289 (1989).
[34] R. Littke, D. R. Baker, and D. Leythaeuser, Org. Geochem. **13**, 549 (1988).